A multichannel magnetic probe system for analysing magnetic fluctuations in helical axis plasmas

S. R. Haskey, B. D. Blackwell, B. Seiwald, M. J. Hole, D. G. Pretty, J. Howard, and J. Wach

Citation: Review of Scientific Instruments **84**, 093501 (2013); doi: 10.1063/1.4819250
View online: http://dx.doi.org/10.1063/1.4819250
View Table of Contents: http://scitation.aip.org/content/aip/journal/rsi/84/9?ver=pdfcov
Published by the AIP Publishing

A multichannel magnetic probe system for analysing magnetic fluctuations in helical axis plasmas

S. R. Haskey, B. D. Blackwell, B. Seiwald, M. J. Hole, D. G. Pretty, J. Howard, and J. Wach
Plasma Research Laboratory, Research School of Physical Sciences and Engineering, The Australian National University, Canberra, ACT 0200, Australia

(Received 15 May 2013; accepted 12 August 2013; published online 3 September 2013)

The need to understand the structure of magnetic fluctuations in H-1NF heliac [S. Hamberger *et al.*, Fusion Technol. **17**, 123 (1990)] plasmas has motivated the installation of a sixteen former, tri-axis helical magnetic probe Mirnov array (HMA). The new array complements two existing poloidal Mirnov arrays by providing polarisation information, higher frequency response, and improved toroidal resolution. The helical placement is ideal for helical axis plasmas because it positions the array as close as possible to the plasma in regions of varying degrees of favourable curvature in the magnetohydrodynamic sense, but almost constant magnetic angle. This makes phase variation with probe position near linear, greatly simplifying the analysis of the data. Several of the issues involved in the design, installation, data analysis, and calibration of this unique array are presented including probe coil design, frequency response measurements, mode number identification, orientation calculations, and mapping probe coil positions to magnetic coordinates. Details of specially designed digitally programmable pre-amplifiers, which allow gains and filters to be changed as part of the data acquisition initialisation sequence and stored with the probe signals, are also presented. The low shear heliac geometry [R. Jiménez-Gómez *et al.*, Nucl. Fusion **51**, 033001 (2011)], flexibility of the H-1NF heliac, and wealth of information provided by the HMA create a unique opportunity for detailed study of Alfvén eigenmodes, which could be a serious issue for future fusion reactors. © *2013 AIP Publishing LLC*. [http://dx.doi.org/10.1063/1.4819250]

I. INTRODUCTION

Magnetic coil probe arrays (Mirnov arrays) are an integral part of the diagnostic suites installed on stellarators and tokamaks.[3–6] They are routinely used to determine the frequency, mode numbers, polarisation, and growth rates of plasma perturbations such as shear and compressional Alfvén waves in the kHz to MHz range. This valuable information is also used to infer underlying plasma parameters.[7,8] Additionally, the raw output of the probes can provide a low latency input to control systems, and supply frequency locking information to other diagnostics.

A single magnetic probe only provides spectral information. To obtain spatial information, such as mode numbers, arrays of probes are used, encoding spatial information in the phase differences between probe signals. In toroidal geometry, separate arrays are often arranged in the toroidal and poloidal directions because these are two natural periodic directions for the decomposition of mode numbers. On helical axis plasmas, a toroidal placement is difficult, and in many cases may be impossible due to access issues. A helical array offers an attractive alternative that provides both toroidal and poloidal mode number information as well as advantages such as minimal and relatively constant distance to the plasma.

The H-1NF heliac[1,2] is a three field-period helical axis stellarator with major radius $R = 1\,\mathrm{m}$ and average minor radius $\langle r \rangle \approx 0.2\,\mathrm{m}$. The design of the machine allows access to an extensive range of magnetic configurations, making H-1NF well-suited to explore the relationship between plasma behaviour and magnetic configuration.[9] A substantial variety of magnetic fluctuations have been observed with two existing poloidal Mirnov arrays (PMAs) in RF heated H/He plasmas.[10,11] Analysis using the existing arrays is difficult due to the lack of toroidal mode number information caused by toroidal under sampling and substantial variation in the distance from the array to the plasma. The probes which are further away from the plasma have significantly smaller signals and a very low signal to noise ratio, provide a less localised measurement, and the additional distance to the plasma increases the uncertainty in the probe's magnetic coordinates. These uncertainties motivated the installation of a new helical array to provide additional toroidal and poloidal mode number information, polarisation information, and higher frequency response.

The helical Mirnov array (HMA) consists of 16 tri-axis magnetic probes (48 probe coils), which follow the helical winding of H-1NF through one of its three revolutions. This places the array as close as possible to the plasma in areas where strong probe signals have been experimentally observed. The relatively equal spacing of the probes allows better mode separation using singular value decomposition (SVD) analysis. An overview of H-1NF including the location of the HMA and poloidal Mirnov arrays are shown in Figures 1 and 2. A single tri-axis probe is shown in Figure 3. The array is encased in a thin stainless steel bellows to minimise attenuation, provide vacuum integrity, and minimise vacuum seal breaks for cabling. The frequency response of the probes inside the bellows is maximised around 100 kHz or 400 kHz depending on probe orientation. Pre-amplifiers with digitally

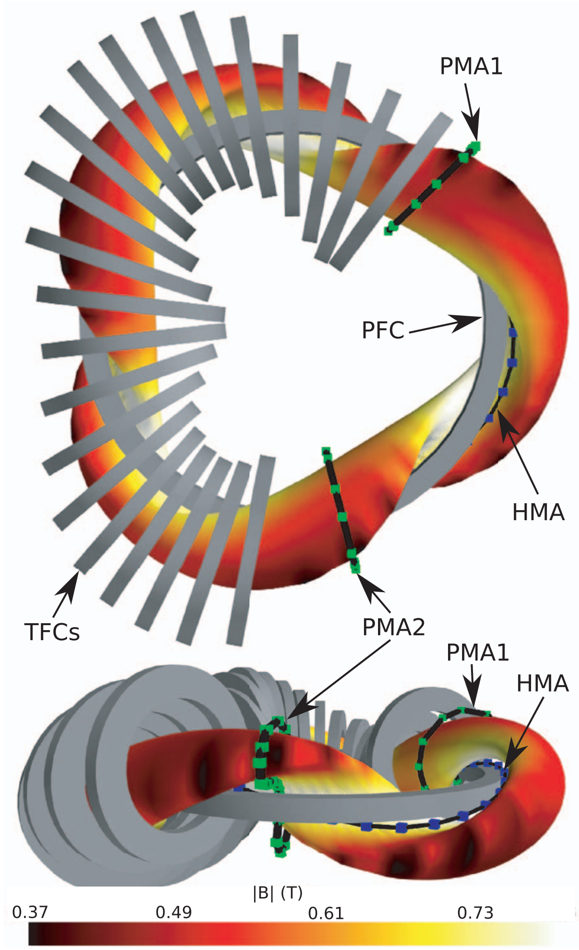

FIG. 1. An overview of the H-1NF heliac showing a subset of the equilibrium magnetic field coils including the poloidal field coil (PFC) and toroidal field coils (TFCs). The locations of the two existing poloidal Mirnov arrays (PMA1 and PMA2) are marked with green cubes, and the helical Mirnov array (HMA) is marked with blue cubes. The last closed flux surface for a particular H-1NF configuration is shown, with the surface color representing the magnitude of the equilibrium magnetic field.

switchable filters and gain allow settings for each shot to be easily modified and stored.

This paper is organised as follows. Section II covers the vacuum considerations, stainless steel bellows housing, probe design, signal amplification, and data acquisition systems. Section III describes the location of the magnetic probes in real space and magnetic coordinates as well as probe orientation calculations. Finally, in Sec. IV, we discuss some of the recent results from the array.

II. ARRAY DESIGN AND SPECIFICATIONS

A. Array housing and vacuum considerations

The H-1NF structure including most magnetic field coils is housed inside a large stainless steel vacuum vessel. Any diagnostic that needs to be placed near the plasma, such as magnetic probes, must be placed inside the vacuum vessel and will be subject to vacuum conditions, imposing considerable constraints on the diagnostic. The decision was made in the early stages of the design to place the array inside a vacuum tight housing allowing the inside of the housing to be at atmospheric pressure. This has several advantages including protection from the plasma, fewer mounting points to the H-1NF structure, simplified cable routing, one vacuum feed-through for all cabling, and the ability to use non-vacuum compatible materials for the probe coil construction.

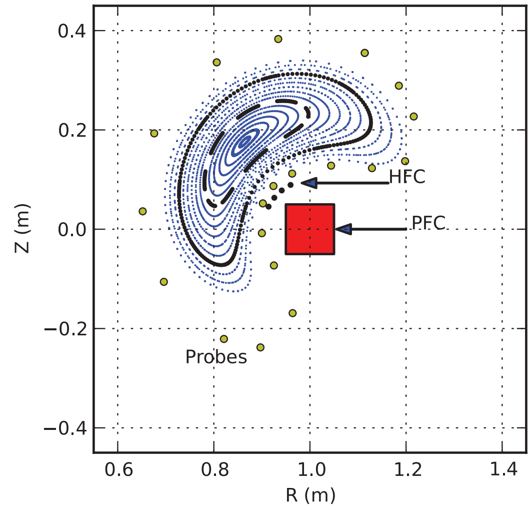

FIG. 2. A Poincaré plot of a poloidal cross-section with the location of the magnetic probes in an existing poloidal array located at a toroidal angle of 44.3°. The locations of the helical field coil conductors (HFC) and poloidal magnetic field coil casing (PFC) are shown along with several flux surfaces for a typical machine configuration. This is for a reversed shear configuration. The closest surfaces to the 4/3 rational surface are marked with black dots. The variable spacing of the probes relative to the plasma causes difficulties in the analysis of the data from this array.

A thin (≈0.26 mm wall thickness) austenitic stainless steel bellows was chosen for the housing due to its flexibility (must be able to follow a helical path), low magnetic permeability, ability to withstand sputtering by the plasma, good vacuum properties, and low conductance relative to other metallic options. The bellows provides electrostatic shielding as well as some magnetic shielding at higher frequencies. The effect this has on the overall frequency response of the system is discussed in Sec. II B.

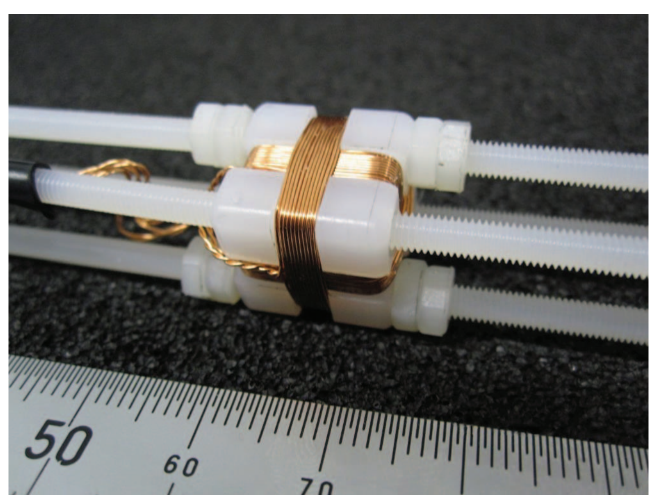

FIG. 3. One of the sixteen tri-axis magnetic probes. The probe coils are wound onto a nylon former. All formers are located on threaded nylon shafts, maintaining their spacing when the array is placed inside the stainless steel bellows housing, shown in Figure 5.

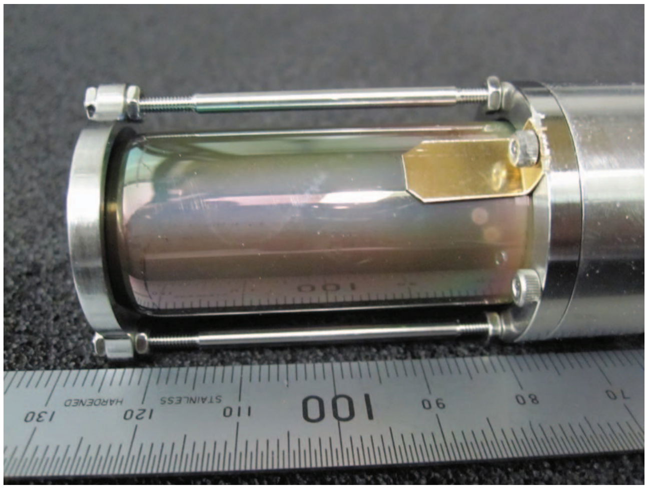

FIG. 4. The last former in the HMA is enclosed inside a copper sputtered borosilicate tube instead of the bellows. This increases the frequency response of the probes, while still providing electrostatic shielding.

Nichrome wire attaches the bellows to mounts, located next to the helical field coil (HFC). Nichrome maximises the resistance of the HMA mounting structure, minimising the effect on the frequency response. At the end of the bellows, a copper sputtered borosilicate tube, shown in Figure 4, houses the final probe in the array. The copper sputtering provides electrostatic shielding, but is thin enough to prevent attenuation of the magnetic field at higher frequencies. Consequently, this probe has a higher frequency response, and can be used to calibrate the effect of the bellows on the response of the other probes. The installed array is shown in Figure 5.

The bellows has an internal diameter of 20.8 mm and an external diameter of 25.8 mm allowing a ≈14 mm cube shaped former to fit comfortably inside the bellows. The maximum size probe coil that can be wound onto this former has a square 12 mm × 12 mm face. Using a cube shaped former centralises the probe coils, and leaves room on the sides of the former to route the twisted pair cables to the other probes.

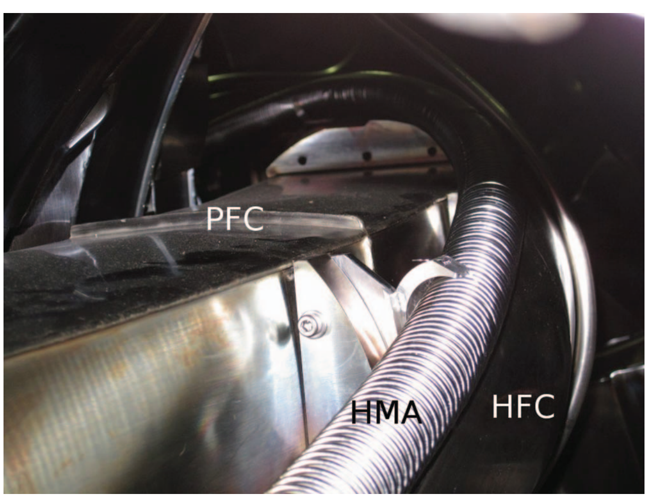

FIG. 5. The installed HMA housed in the stainless steel bellows. The array is attached to the side of the helical magnetic field coil (HFC) causing it to follow a helical path and wrap around the poloidal field coil (PFC).

B. Probe design and frequency response

The magnetic probe formers are made from nylon whose heat resistance is too low for long pulse high temperature machines. H-1NF has short pulses (≈100 ms), so the heat load on the formers is low. Two temperature sensors, which monitor the temperature near the formers, have confirmed that the temperatures near the formers remain below 30 °C.

The magnetic probe dimensions are greatly constrained by the bellows housing; however, selecting the number of turns on the probe coils allows us to optimise the frequency response for our application. Ideally, the probes should produce as large an output as possible to minimise the pre-amplification required and have a high frequency response. Unfortunately, these requirements conflict with one another and compromises must be made. Based on observations from the existing PMAs,[10,11] magnetic fluctuations exist up to 150 kHz. Additionally, theoretical modelling has shown the existence of significant Alfvén continuum gaps in the low hundreds of kHz range[12,13] suggesting we want the frequency response to be maximum at these frequencies.

As discussed in Ref. 4, the voltage output of a magnetic probe up to its first self resonant frequency can be modelled by $V(\omega) = -j\omega NAB_c(\omega)$. Here, $j^2 = -1$ and N, A, $B_c(\omega)$, and ω represent the number of turns, probe area, magnetic fluctuation amplitude, and frequency of the oscillation, respectively. The probe can be modelled as a RLC circuit where R_c, L_c, and C_c represent probe resistance, self inductance, and stray capacitance, respectively. A transmission line with impedance Z_0 can be included to model the effect of the cabling from the probe to the pre-amplifiers. The voltage across a terminating resistor (R_t) is used as the input to pre-amplifiers or digitisers. A schematic of this lumped circuit element model is shown in Figure 6(a). Impedance matching between the digitiser or pre-amplifier and the transmission line is achieved by setting $R_t = Z_0$. This prevents reflections and allows us to eliminate the transmission line from the model, reducing the circuit to the simple RLC circuit shown in Figure 6(b). This model allows us to easily calculate the self resonant frequency and −3 dB point of the probe once L_c and C_c, and Z_0 are known.

A trade-off exists between high frequency response and probe output at lower frequencies. The cutoff frequency of

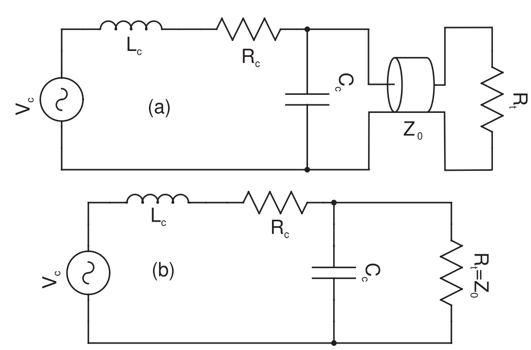

FIG. 6. (a) A lumped circuit element representation of a magnetic probe, transmission line, and terminating resistor. (b) Setting the terminating resistance to match the impedance of the transmission line allows us to model the system using a simpler RLC circuit.

TABLE I. Measured parameters for magnetic probes with 11, 22, and 33 turns representing single, double, and triple layer probes. The −3 dB point assumes termination into 60 Ω, matching the impedance of the twisted pair transmission line.

Parameter	11 turns	22 turns	33 turns
R_p (mΩ)	110	220	340
L_p (μH)	2.8	10	22
C_p (pF)	1.3	17	17
F_r (MHz)	82.0	12.3	8.5
NA (cm^2)	15.8	31.7	47.5
−3 dB (kHz)	3400	960	430

the probe is constrained by the probe inductance which increases with N^2A, while the probe output at lower frequencies increases with $N A$. Therefore, to maximise the probe output at lower frequencies, while still maintaining as high a cutoff frequency as possible, we want to maximise the area of the probe within the constraints imposed by the internal diameter of the bellows housing. Therefore, we choose a square shaped coil with a side length of 12 mm, which maximises the use of the available area, allows room for routing cables past the probe, and leaves the number of coil turns as a free variable. The choices shown in Table I correspond to single, double, and triple layer windings using AWG30 enamelled copper wire, which was the thinnest wire that could reliably withstand the possible stresses during the installation of the array. The measured probe resistance, self inductance, and stray capacitance of each of these options, along with the calculated −3 dB point and first resonant frequency are shown.

The 22 turn probe was chosen as the best compromise between low frequency probe output (NA) and cutoff frequency. The 11 turn probe provides an unnecessarily high cutoff frequency when the effect of the bellows is taken into account, and the 33 turn probe does not provide a high enough cutoff. The double layer winding offers additional benefits such as having the transmission line leads line up, and cancellation of the off-normal sensitivity due to the slight winding pitch.

The magnetic probes are located roughly 6 m from the pre-amplifiers and are connected using a twisted pair transmission line. The probe coils and transmission line are constructed from a single length of enamelled copper wire. This improves the reliability of the system by eliminating joins, and removes impedance changes that could cause signal reflections. The impedance of the transmission line was measured by time domain reflectometry as 60 Ω and the terminating resistor was chosen to match this. Additionally, the length of each transmission line is the same for all probes to minimise the effect of slight impedance mismatches with the terminating resistor.

The ribbed shape of the bellows complicates the attenuation of the magnetic field. The ribs cause an increase in the resistivity per unit length for eddy currents flowing axially along the bellows, and a reduction for currents flowing around the bellows. This decreases (increases) the diffusion time for transverse (axial) magnetic fields, which increases (decreases) the high frequency response relative to a plain cylindrical housing with a similar wall thickness. A

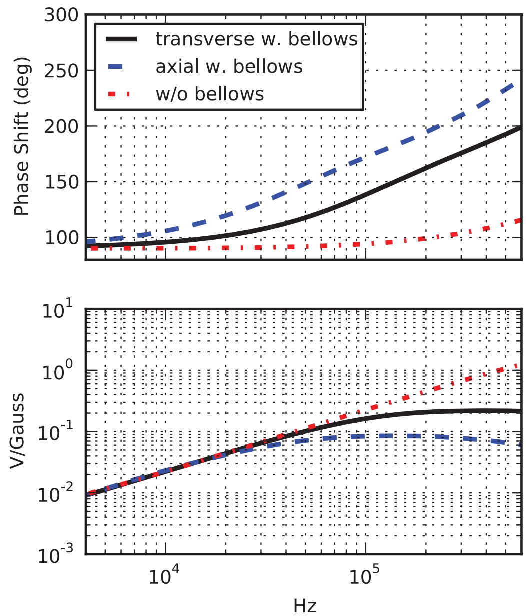

FIG. 7. The measured frequency response of the magnetic probes. The response without the bellows housing is shown—this is valid for the probes in the borosilicate tube. For the rest of the array inside the bellows, the response depends on whether the probe is pointing in the axial or transverse direction.

Helmholtz coil was used to measure the frequency response for the unshielded probe, and the two different orientations inside the bellows. Figure 7 shows the measured frequency response of the magnetic probes. The response of the axially oriented probes is maximised at ≈100 kHz, while the transversely oriented probes response is maximised at ≈400 kHz.

C. Signal amplification and data acquisition

Custom designed programmable pre-amplifiers with several special features increase the probe output to fully use the dynamic range of the digitisers. The probe output varies considerably depending on the plasma conditions and magnetic configuration.[9,14] Therefore, it is necessary to have several different gain settings that prevent the pre-amplifiers from clipping, while providing sufficient pre-amplification of the signal for the digitisers. Discrete gain settings of ≈125, 250, 625, and 1250 were chosen based on the analysis of the probe data from the existing magnetic probes and data from prototype pre-amplifiers.

In addition to providing gain, the pre-amplifiers include several passive and active filters to minimise the contribution from several unwanted signals such as high frequency pickup from the 5-8 MHz RF heating system, which is aliased due to the 2 MHz sampling rate, and low frequency field coil power supply switching noise. The impulse switching noise from the magnetic field coil power supplies is very weak as seen in Figure 14 and depends on their current output; however, the frequency is usually 2 or 2.4 kHz, with weaker harmonics at 4 and 6 kHz. There is also some ripple in the magnetic field coil currents. The field coil power supplies have a ripple of ≈1 A at 10 Hz, except for the secondary power supply which has a ripple of ≈20 A at 30 Hz when supplying the helical winding alone. All active filters and gain settings can be manually or

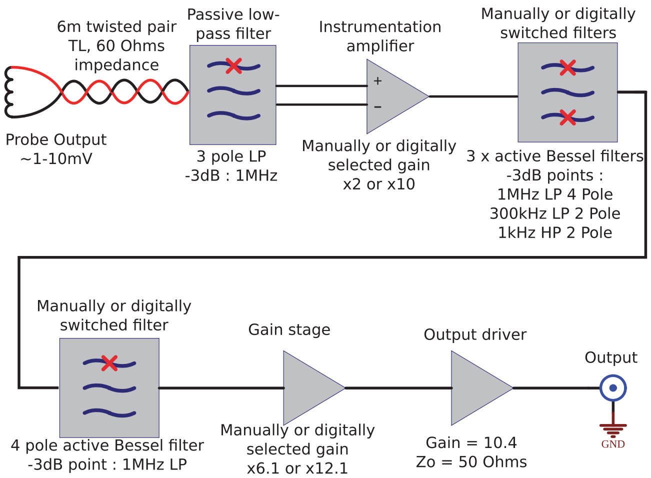

FIG. 8. Block diagram of the pre-amplifiers illustrating the various stages and the overall signal path.

digitally controlled (or bypassed) providing a high degree of flexibility.

The pre-amplifier gain and filter stages are shown in Figure 8. The probe signal passes through a three pole low pass passive filter with a −3 dB point of 1 MHz. This prevents overloading the first stage of the pre-amplifier with pickup from the RF plasma heating. The signal then passes through an instrumentation amplifier (Analog Devices AD8250) providing the first adjustable gain stage (×2 or ×10), converting the balanced signal to single ended and buffering the signal for the following stages. Following this, the signal passes through two active low pass (LP) and one active high pass (HP) filters, all of which are Bessel filters (for optimal phase response) with −3 dB points of 1 MHz (LP 4 pole), 300 kHz (LP 2 pole), and 1 kHz (HP 2 pole), respectively. The signal then passes through a 4 pole low pass Bessel filter with a 1 MHz −3 dB point before passing through another gain stage (AD8034) with gain selections of ×6.1 or ×12.1 and an output driver stage with a gain of ×10.4 (AD8397). The second 1 MHz low pass filter is included before the major gain stages for situations when the pickup from the RF plasma heating system is exceptionally large. The active filters are implemented using unity gain Sallen-Key designs. A picture of a pre-amplifier is shown in Figure 9(b).

It is possible that certain probes may require different gain and filter settings for the same shot due to their different locations and orientations. Given the large number of probes and the difficulty in manually recording or changing all of the settings for each shot, all pre-amplifier settings are digitally controlled (with the option for manual override). This allows the settings to be chosen before a shot, transmitted to the pre-amplifiers, and recorded with the shot data. All of this happens automatically as part of the H-1NF initialisation and store phases for each shot, and allows the effect of the pre-amplifier settings on the signal to be accounted for in the post shot processing.

Digital switching of the gain and filters is implemented using ADG714 analog switches connected via a buffered serial peripheral interface bus (SPI) interface, run by a microcontroller. The pre-amplifiers are connected to a backplane

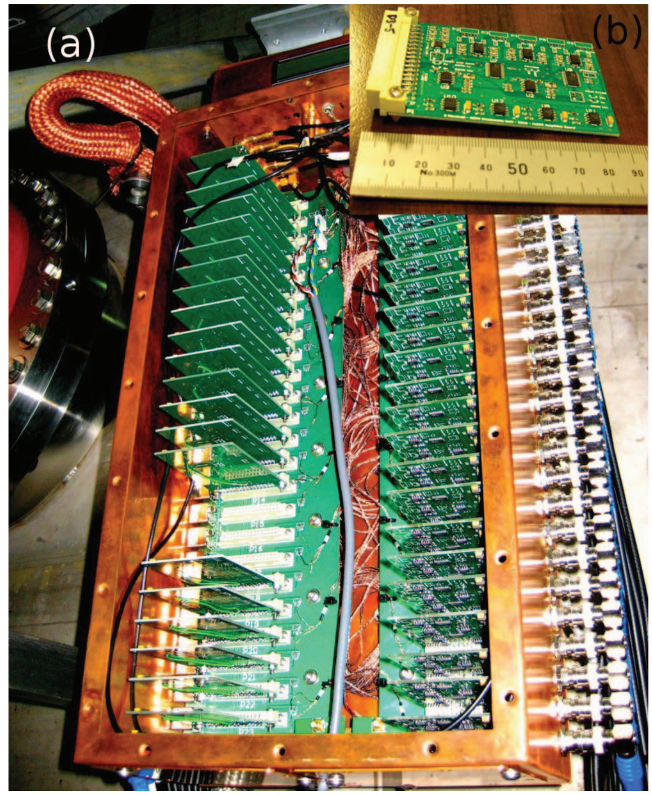

FIG. 9. (a) The 48 pre-amplifiers housed in a copper box, and installed on backplanes to allow communication signals for the digital switching of filters and gains. Three amplifiers have been removed to show the backplane. (b) A single pre-amplifier.

allowing the boards to access the control signals. All pre-amplifiers are placed inside a copper housing, shown in Figure 9(a), to prevent unwanted pickup from a nearby high power RF matching box. The pre-amplifier output is usually digitised at 2 MHz using D-TACQ ACQ132 digitisers with the option to digitise the higher frequency response probes at 16 MHz or 32 MHz. In the higher frequency case, the pre-amplifiers are bypassed and the raw Mirnov signal is acquired. The Mirnov signals are recorded in an MDSplus database[15] along with the pre-amplifier settings. Automatic storage of the pre-amplifier settings simplifies data analysis and eliminates errors that can occur with manual record keeping.

III. ARRAY POSITIONING AND ORIENTATION CALCULATIONS

A. Probe locations in real space and magnetic coordinates

The HMA is placed alongside the helical field coil in H-1NF as shown in Figures 5 and 10, locating the probes as close as possible to the plasma. The variation of the radial position of the probes with toroidal angle, relative to the plasma, is small simplifying the analysis of the signals compared with the PMA (Figure 2). While it is possible to vary the toroidal spacing of the probes to maximise the mode resolving power of the array,[4] this was not done because there was uncertainty in the final installed location of the probes when the array was manufactured and equal spacing of probes is in general more

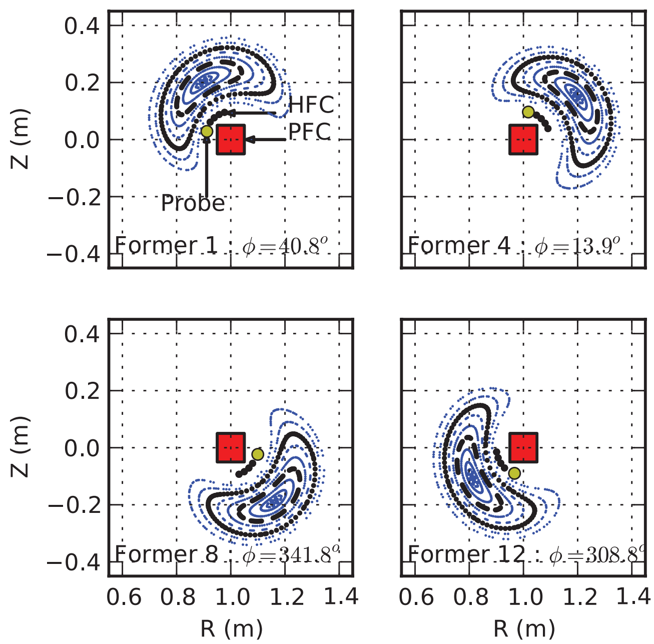

FIG. 10. Poincaré plots of the poloidal cross-sections for a typical H-1NF configuration at the toroidal location (ϕ) of selected probes in the HMA, marked by yellow circles, illustrating their proximity to the plasma. The helical field coil (HFC) and poloidal field coil (PFC) are also shown. This is for a reversed shear configuration. The closest surfaces to the 4/3 rational surface are marked with black dots.

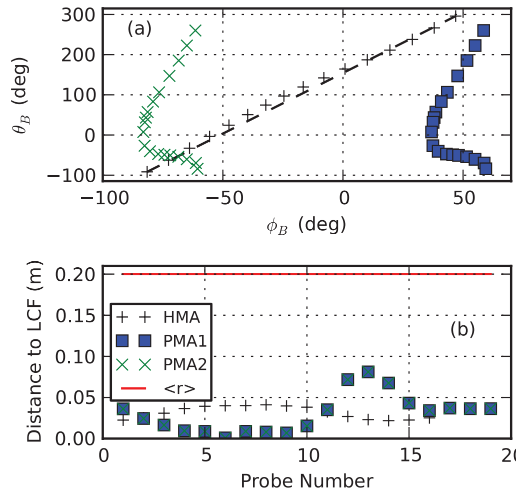

FIG. 11. (a) Probe locations in Boozer coordinates for the two poloidal Mirnov arrays (PMA1, PMA2) and the helical Mirnov array (HMA), based on the closest location on the last closed flux surface for a typical H-1NF magnetic configuration. The probes in the HMA follow an almost straight path (marked by the dashed line) in (θ_B, ϕ_B) space. (b) Distance from the probes to the nearest point on the last closed flux surface. The plasma average minor radius is included for comparison. The distance for the HMA is small and relatively constant along the array, while the distance for the PMAs varies considerably between probes. PMA1 and PMA2 have identical construction and their toroidal location is offset by one field period which is why they overlay.

insensitive to probe failure than uneven spacing. The probes have a 15.6 cm spacing along the helical path of the bellows, which is controlled by threaded nylon rods that connect the probes to one another (Figure 3). This causes a slight bunching up (in toroidal angle) of the probes on the outside of the poloidal field coil (PFC), and a stretching on the inside.

When analysing the array outputs to determine mode numbers, the location of the magnetic probes needs to be mapped to a coordinate system where the magnetic field lines follow straight lines. One such coordinate system for the fully three-dimensional plasmas produced in H-1NF is the Boozer coordinate system (s, θ_B, ϕ_B).[16,17] Here, s is closely related to a radial variable squared, while θ_B and ϕ_B are angle like variables similar to poloidal and toroidal coordinates, respectively. Transformation of the probe coordinates in real space to Boozer coordinates is not simple as Boozer coordinates are not defined at the probe locations since they are outside the last closed flux surface (LCFS). To overcome this problem, we map the real space location of the probes to their nearest point on the LCFS, and transform this location into Boozer coordinates. The mapping of the probes' locations is particularly useful because it allows comparisons with the predicted eigenfunctions from codes such as CAS3D.[18,19] The VMEC code[20] solves the plasma equilibrium, which is used for the coordinate transformation. The BOOZ_XFORM code (part of the STELLOPT package, which includes VMEC) uses this equilibrium to provide the transformation to Boozer coordinates.

The location of the helical and poloidal arrays in Boozer coordinates for a particular magnetic configuration is shown in Figure 11(a). Although not shown for clarity, the location of the probes varies slightly for different magnetic configurations. This is taken into account when analysing data from different configurations. The HMA follows an almost straight line in (θ_B, ϕ_B) space allowing the array to provide toroidal and poloidal mode number information which is relatively easy to analyse. The almost equal spacing of the probes allows better mode separation using SVD analysis. Figure 11(b) shows how the distance to the nearest point on the LCFS changes along the arrays demonstrating the consistent spacing for the HMA compared with the PMAs. Additionally, Figure 11(a) clearly shows how the HMA provides toroidal information that is missing from the PMAs.

The probe output to a mode that consists of dominantly one component such as a global Alfvén eigenmode[21] can be described as follows:

$$V_i \propto \cos(n\phi_{B,i} + m\theta_{B,i} - \omega t).$$

Here, n represents the toroidal mode number, m the poloidal mode number, ω is the mode frequency, i an index for the toroidally successive probes, and $\phi_{B,\,i}$ and $\theta_{B,\,i}$ are the toroidal and poloidal Boozer angles of the ith probe, respectively. Using this representation, we can simulate the phase difference at the frequency of interest (ω), between toroidally successive probe ($D(n, m, i)$) and the cumulative phase along the array up to the jth probe (C_j) as follows:

$$D(n,m,i) = n(\phi_{B,i} - \phi_{B,i-1}) + m(\theta_{B,i} - \theta_{B,i-1}), \qquad (1)$$

$$C_j = \begin{cases} 0 & \text{for } j = 0 \\ \sum_{i=2}^{j+1} D(n,m,i) & \text{for } 1 \le j \le n_p - 1 \end{cases}, \qquad (2)$$

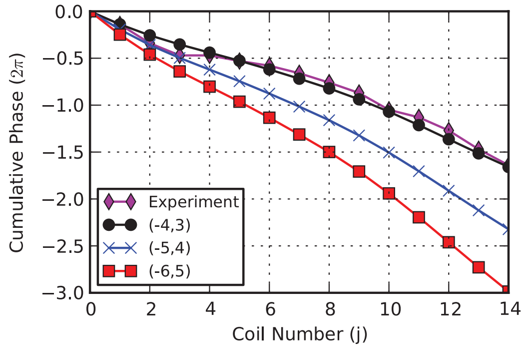

FIG. 12. Simulated cumulative phase, C_j (Eq. (2)), for three different modes in Boozer coordinates. An experimentally obtained mode that is a close fit to ($n = -4$, $m = 3$) is shown. The spectrogram and time traces for the experimental data are shown in Figures 14 and 15.

where n_p is the number of probes in the array. Figure 12 shows the simulated values of C_j for several mode numbers demonstrating how the HMA can be used to identify mode numbers. The experimentally obtained cumulative phase for a mode that was identified using SVD techniques[11] is also shown. A spectrogram and time varying traces from the probes for this particular mode are shown in Figures 14 and 15 in Sec. IV. In this case, the experimental data are a close fit to a ($n = -4$, $m = 3$) mode.

One of the difficulties of analysing data from the HMA is that certain mode numbers are difficult to differentiate from one another if

$$n_1 + (\Delta\theta_{B,i}/\Delta\phi_{B,i})m_1 = n_2 + (\Delta\theta_{B,i}/\Delta\phi_{B,i})m_2, \qquad (3)$$

where $\Delta\theta_{B,i} = (\theta_{B,i} - \theta_{B,i-1})$ and $\Delta\phi_{B,i} = (\phi_{B,i} - \phi_{B,i-1})$. This can be obtained from Eq. (1) by setting $D(n_1, m_1, i) = D(n_2, m_2, i)$. For the HMA, $\Delta\theta_{B,\,i}/\Delta\phi_{B,\,i} \approx 3$ for all i, which means that the phase of two modes satisfying $n_1 + 3m_1 = n_2 + 3m_2$ will look similar. The reason they do not look identical is because $\Delta\theta_{B,\,i}/\Delta\phi_{B,\,i}$ varies slightly between pickup coils. For example, a ($n = -4$, $m = 3$) mode will look similar to any other modes where $n + 3m = 5$ such as (-1, 2) or (2, 1). Therefore, information from the HMA should be supplemented with other information such as data from the PMAs to provide more confidence in the mode numbers. While the HMA provides information about both toroidal and poloidal mode numbers, analysis is more complicated than for separate toroidal and poloidal arrays.

B. Probe orientation calculations

The orientation of the three probes on all 16 formers must be calculated after installation because the formers are free to rotate, within limits, inside the bellows during installation. A dominantly 4 Hz, 50 A current was applied individually to the five magnetic field coil sets (outer vertical coils (OVC), inner vertical coils (IVC), helical coil (HFC), toroidal coils (TFC), and poloidal coil (PFC)) and the probe outputs due to these fields were integrated and recorded. The HELIAC code[22,23] was used to calculate the applied magnetic field corresponding to each of the probe measurements. Using this information, we calculated the orientation of the probes using two different methods: the preferred method, which is based on Euler rotations and assumes that the probes are orthogonal, and a second method, which solves for the orientations directly, but does not enforce that the probes are orthogonal to one another. These methods are described and compared below.

We start by defining a matrix, $\mathbf{N}$, for each tri-axis magnetic probe, describing the orientations of the three probe coils on a tri-axis probe. The directions normal to the faces of the probe coils, $\hat{\mathbf{n}}_1$, $\hat{\mathbf{n}}_2$, and $\hat{\mathbf{n}}_3$, are represented as follows:

$$\mathbf{N} = \begin{bmatrix} \hat{\mathbf{n}}_1 \\ \hat{\mathbf{n}}_2 \\ \hat{\mathbf{n}}_3 \end{bmatrix} = \begin{bmatrix} n_{1,x} & n_{1,y} & n_{1,z} \\ n_{2,x} & n_{2,y} & n_{2,z} \\ n_{3,x} & n_{3,y} & n_{3,z} \end{bmatrix} \begin{bmatrix} \hat{\mathbf{x}} \\ \hat{\mathbf{y}} \\ \hat{\mathbf{z}} \end{bmatrix}, \qquad (4)$$

where $\hat{\mathbf{x}}$, $\hat{\mathbf{y}}$, and $\hat{\mathbf{z}}$ represent the standard Cartesian coordinate basis vectors.

The integrated probe output due to the field created by one of the equilibrium field coil sets can be represented in the following matrix, $\mathbf{V} = [V_{p,f}]$. Here p represents one of the three probe coils on a tri-axis probe and f represents the magnetic field coil set responsible for generating the measurement (OVC, PFC, IVC, HFC, or TFC). The applied magnetic field, which generated these measurements, is calculated by HELIAC and can be represented in the following matrix, $\mathbf{B} = [B_{a,f}]$, where a represents the components of the applied field in the $\hat{\mathbf{x}}$, $\hat{\mathbf{y}}$, or $\hat{\mathbf{z}}$ direction. We normalise the measurements and applied field ($\sum_p (V_{p,f})^2 = 1$ and $\sum_a (B_{a,f})^2 = 1$) to remove the effect of the probe and integrator responses.

Representing $\mathbf{N}$ as a rotation matrix, which is constructed using Euler rotations, enforces that the probes on a single former are orthogonal to one another. For any given set of Euler rotations, the predicted probe outputs are given by $\mathbf{Z} = \mathbf{NB}$. A measure of the error between the predicted probe outputs and measured outputs is given by

$$E = \sqrt{\sum_{p,f} ((Z_{p,f} - V_{p,f})^2)/n_f}, \qquad (5)$$

where n_f is the number of separate field coils used for the measurements. We can find the Euler rotations, and consequently, $\mathbf{N}$ that minimises E using standard minimisation techniques. This is then chosen as the correct orientation of the probe coils on the tri-axis former. An approximation of the orientation error in the calculation is given by $\arcsin(E)$. This orientation error is shown in Figure 13 for all of the tri-axis formers, demonstrating a maximum rms error of $\approx 6^\circ$.

An alternate and less preferred method in this situation is to remove the assumption of orthogonality and solve for the probe orientations directly. Representing the probe outputs to the various fields, $\mathbf{V} = \mathbf{NB}$, allows us to calculate the probe orientations, $\mathbf{N} = \mathbf{VB}^{-1}$. If we include more than three separate field coil sets in the calculation, the solution can be found using the pseudo inverse of $\mathbf{B}$. The accuracy of the result can be checked by comparing how close to 90° the angles between $\hat{\mathbf{n}}_1$, $\hat{\mathbf{n}}_2$, and $\hat{\mathbf{n}}_3$ are. These angles (three per tri-axis probe) are shown in Figure 13 for all the tri-axis probes.

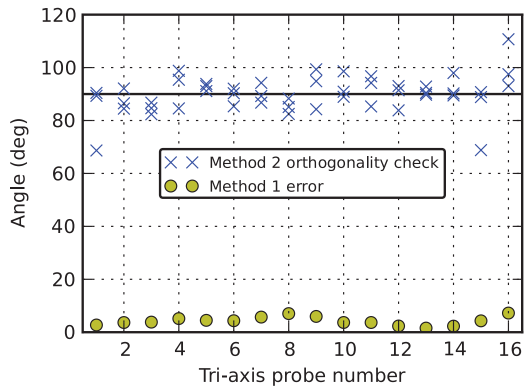

FIG. 13. The orientation error from the Euler rotation method (method 1) is approximated using arcsin(E) where E is defined in Eq. (5). The angles between $\hat{\mathbf{n}}_1$, $\hat{\mathbf{n}}_2$, and $\hat{\mathbf{n}}_3$ on a tri-axis former are used as an orthogonality check for the second method (three possible angles can be calculated for each tri-axis probe).

Both methods produce similar results for many of the probes; however, the first method (Euler rotation method), which enforces the orthogonality of the probes, is preferred, as this is known to be the case to high accuracy and provides additional information for the calculation. This extra information is particularly important if the fields from several field coil sets have similar directions at the probe location, which is the case for probes 1 and 15 in Figure 13. This similarity (or degeneracy) causes the second method to incorrectly imply that the probes on two formers are as far as 20° off normal which is known to be false. However, in situations, where it is possible to apply sufficiently different fields, both methods give the same result, and the second method is substantially faster.

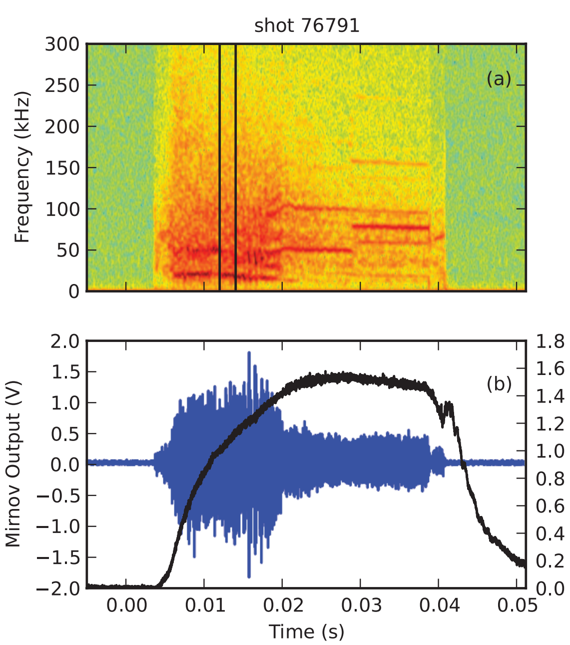

FIG. 14. (a) Spectrogram of one probe output during a shot. Analysis of the ≈20 kHz mode between the two vertical bars is shown in Figures 12 and 15. (b) Raw time signal output from the pre-amplifiers (blue) and line averaged electron density trace (black).

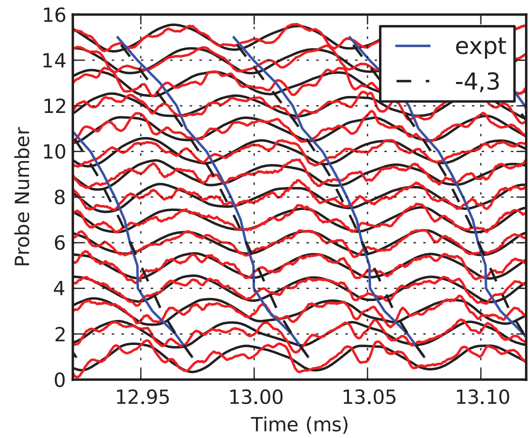

FIG. 15. The raw probe signals for the axially oriented probes are plotted in red. SVD is used to identify the dominant component. Band-pass filtering around the dominant component's frequency creates the black traces. The blue diagonal line marks the same phase in the dominant frequency and clearly illustrates the phase difference in the probe signals at the frequency of interest. Also shown is the expected phase difference for a ($n = -4$, $m = 3$) mode showing a good fit. The cumulative phase across the array for these data is shown in Figure 12.

IV. RESULTS

The initial results from the HMA have been very promising with a large variety of magnetic fluctuations being observed. An example of strong mode activity in the spectrogram from a magnetic probe is shown in Figure 14(a). This particular shot was for a reversed shear magnetic configurations which contains 4/3 rational surfaces whose location is shown in Figures 2 and 10.

The array has been successful in identifying mode numbers. Analysis of the ≈20 kHz signal between the two vertical bars in Figure 14(a) gives the experimentally obtained cumulative phase shown in Figure 12. Comparison with the simulated mode numbers shows that in this case, a ($n = -4$, $m = 3$) mode is clearly the best fit. Previously, using just information from the PMAs, there was a great deal of uncertainty in n. This particular mode was identified using SVD techniques.[11] The raw probe signals from this mode are plotted in Figure 15. Also shown in Figure 15 are the probe signals passed through a digital band-pass filter centered on the mode frequency (as obtained from the SVD analysis). The diagonal lines mark the same phase in the signals illustrating the clear phase difference in the signals between probes along the array, which provides spatial information about the mode and confirms the mode numbers.

V. CONCLUSION

Many of the uncertainties in the spatial information of magnetic fluctuations in H-1NF helical axis plasmas have been resolved with the installation of a helical Mirnov array. Figure 1 shows that the array follows the helical winding of H-1NF through one of its three revolutions, placing it as close as possible to the plasma, which results in larger more uniform amplitudes compared with the PMAs. The new array complements two existing poloidal Mirnov arrays by providing polarisation information, higher frequency response, and toroidal resolution. The location of the probes in magnetic coordinates is shown to be near linear with almost equal probe spacing. This makes phase variation with probe position approximately linear, greatly simplifying the analysis of the spatial nature of the modes and allowing better mode separation using SVD analysis.

Calibration of the frequency response, orientation, and position of the array in real and magnetic coordinates has been presented. The effect of the thin stainless steel bellows, which surrounds the array, has been measured and reduces the maximum frequency response to ≈400 kHz or ≈100 kHz depending on the orientation of the probe within the bellows. A single former, placed inside a copper sputtered borosilicate tube, has provided useful signals up to 7 MHz. Two methods for calculating the orientation of the probes using the equilibrium magnetic field coil sets provide complimentary and crosschecking information. Additionally, details of the mapping of the coil locations to magnetic coordinates, based on the nearest location on the last closed flux surface were presented. Pre-amplifiers with digitally switchable filters and gain settings, developed for the HMA, have performed very well under expected conditions. Data analysis confirms that the pre-amplifier settings are controlled reliably for each shot and recorded along with the digitised signals in a MDSplus database, simplifying data analysis and eliminating record keeping errors.

In summary, initial results from the HMA have been very promising, with it performing as designed. The array successfully provides information which is crucial for identifying mode numbers and determining the spatial nature of the observed fluctuations. The higher frequency response, polarisation information, and improved toroidal resolution of the HMA combined with the flexibility of the H-1NF heliac will allow the observed waves dependence on parameters, such as magnetic field geometry, density, and heating power to be explored in great detail.

ACKNOWLEDGMENTS

The authors would like to thank the H-1NF team for continued support of experimental operations. The RSPE Electronics Unit, and Steven Marshall in particular, contributed a great deal towards the pre-amplifier design and construction. This work was supported by the Education Investment Fund under the Super Science Initiative of the Australian Government. S.R.H. wishes to thank AINSE Ltd. for providing financial assistance to enable this work on H-1NF to be conducted.

[1] S. Hamberger, B. Blackwell, L. Sharp, and D. Shenton, Fusion Technol. **17**, 123 (1990).
[2] R. Jiménez-Gómez, A. Könies, E. Ascasíbar, F. Castejón, T. Estrada, L. Eliseev, A. Melnikov, J. Jiménez, D. Pretty, D. Jiménez-Rey *et al.*, Nucl. Fusion **51**, 033001 (2011).
[3] E. Strait, Rev. Sci. Instrum. **77**, 023502 (2006).
[4] M. Hole, L. Appel, and R. Martin, Rev. Sci. Instrum. **80**, 123507 (2009).
[5] R. F. Heeter, A. F. Fasoli, S. Ali-Arshad, and J. M. Moret, Rev. Sci. Instrum. **71**, 4092 (2000).
[6] H. Takahashi, S. Sakakibara, Y. Kubota, and H. Yamada, Rev. Sci. Instrum. **72**, 3249 (2001).
[7] S. Sharapov, D. Testa, B. Alper, D. Borba, A. Fasoli, N. Hawkes, R. Heeter, M. Mantsinen, M. Von Hellermann *et al.*, Phys. Lett. A **289**, 127 (2001).
[8] B. Breizman and S. Sharapov, Plasma Phys. Control. Fusion **53**, 054001 (2011).
[9] J. Harris, M. Shats, B. Blackwell, W. Solomon, D. Pretty, S. Collis, J. Howard, H. Xia, C. Michael, and H. Punzmann, Nucl. Fusion **44**, 279 (2004).
[10] D. Pretty, "A study of MHD activity in the H-1 heliac using data mining techniques," Ph.D. thesis, The Australian National University, 2007.
[11] D. Pretty and B. Blackwell, Comput. Phys. Commun. **180**, 1768 (2009).
[12] J. Bertram, M. Hole, D. Pretty, B. Blackwell, and R. Dewar, Plasma Phys. Control. Fusion **53**, 085023 (2011).
[13] J. Bertram, B. Blackwell, and M. Hole, Plasma Phys. Control. Fusion **54**, 055009 (2012).
[14] B. Blackwell, D. Pretty, J. Howard, R. Nazikian, S. Kumar, D. Oliver, D. Byrne, J. Harris, C. Nuhrenberg, M. McGann *et al.*, preprint arXiv:0902.4728v1 (2009).
[15] T. Fredian and J. Stillerman, Fusion Eng. Des. **60**, 229 (2002).
[16] A. H. Boozer, Phys. Fluids **23**, 904 (1980).
[17] W. D. D'haeseleer, W. N. G. Hitchon, J. D. Callen, and J. L. Shohet, *Flux Coordinates and Magnetic Field Structure: A Guide to a Fundamental Tool of Plasma Structure*, Springer Series in Computational Physics (Springer-Verlag, Berlin, 1991).
[18] C. Schwab, Phys. Fluids B **5**, 3195 (1993).
[19] C. Nührenberg, Phys. Plasmas **6**, 137 (1999).
[20] S. Hirshman and J. Whitson, Phys. Fluids **26**, 3553 (1983).
[21] W. W. Heidbrink, Phys. Plasmas **15**, 055501 (2008).
[22] A. Ehrhardt, *Algorithms for Real Time Magnetic Field Tracing and Optimization* (Princeton Plasma Physics Laboratory, Princeton, NJ, 1985).
[23] B. Blackwell, B. McMillan, A. Searle, and H. Gardner, Comput. Phys. Commun. **142**, 243 (2001).